PHYSICAL REVIEW D **95,** 014503 (2017)

Gribov horizon and Gribov copies effect in lattice Coulomb gauge

Giuseppe Burgio,[*] Markus Quandt,[†] Hugo Reinhardt,[‡] and Hannes Vogt[§]
Institut für Theoretische Physik, Auf der Morgenstelle 14, 72076 Tübingen, Germany
(Received 20 August 2016; published 9 January 2017)

Following a recent proposal by Cooper and Zwanziger, we investigate via $SU(2)$ lattice simulations the effect on the Coulomb gauge propagators and on the Gribov-Zwanziger confinement mechanism of selecting the Gribov copy with the smallest nontrivial eigenvalue of the Faddeev-Popov operator, i.e., the one closest to the Gribov horizon. Although such choice of gauge drives the ghost propagator towards the prediction of continuum calculations, we find that it actually overshoots the goal. With increasing computer time, we observe that Gribov copies with arbitrarily small eigenvalues can be found. For such a method to work, one would therefore need further restrictions on the gauge condition to isolate the physically relevant copies, since, for example, the Coulomb potential V_C defined through the Faddeev-Popov operator becomes otherwise physically meaningless. Interestingly, the Coulomb potential alternatively defined through temporal link correlators is only marginally affected by the smallness of the eigenvalues.

DOI: 10.1103/PhysRevD.95.014503

I. INTRODUCTION

Coulomb gauge plays a prominent role in the Hamiltonian formulation of non-Abelian gauge theories [1–6]; within this framework, variational *Ansätze* offer a promising approach to determine the vacuum state [4,7–9]. In the last years, much effort has been invested in this direction, achieving a large number of interesting analytical results which combine to a rather concise picture of the low-energy sector in gauge theories, see, e.g., Refs. [5,10,11]. The picture of the vacuum conveyed by this approach is the Gribov-Zwanziger (GZ) confinement scenario, which in turn is based on a restriction of the functional integral to the first Gribov region. Applied to Coulomb gauge, this scenario leads to a number of general predictions which are not tied to the variational approach and which can be accessed directly in lattice simulations:

(1) The Coulomb potential should be bound from below [5] by the physical Wilson potential [12], i.e., the presence of Coulomb confinement should be a *necessary* condition for the physical confinement mechanism to take place.
(2) The gluon dispersion relation should be infrared (IR) divergent, naturally providing a confining scale [1].
(3) The Coulomb gauge ghost form factor should be IR-divergent.

The variational approach of Refs. [8–10,13] realizes this scenario, provided that the third condition (often called the *horizon condition* in this context) is implemented as a boundary condition.[1] Therefore, a lattice investigation of the above listed Coulomb gauge correlators represents a powerful tool to gain insight in the mechanism of quark confinement while offering a direct bridge to continuum setups; this program has been thoroughly carried out in Refs. [15–21]. While the gluon sector has been found to agree with the continuum predictions, confirming the dynamical generation of a Gribov mass $M \approx 0.9$ GeV and the validity of Gribov's formula for the gluon propagator [15,16], the ghost sector was shown to agree only qualitatively with the continuum predictions. In particular, the IR divergence of the ghost form factor determined in lattice simulations [19–21] is much weaker than the one predicted by continuum calculations [8,10,13], and a Coulomb string tension could be extracted from the IR behavior of the Coulomb potential only under very optimistic assumptions [19–21]. Furthermore, the lattice results are in conflict with the sum rule for the infrared exponents [10], which merely assumes that the ghost-gluon vertex in Coulomb gauge is bare, or at least nonsingular, in the deep infrared.

In a recent work, Cooper and Zwanziger [22] have proposed to implement Coulomb gauge by picking the Gribov copy with the lowest eigenvalue of the Faddeev–Popov operator, instead of the "best copy" (*bc*) with the maximal value of the Coulomb gauge functional. They argue that a lattice simulation based on such a setup would lead to a better agreement with continuum predictions. The aim of this paper is to directly implement this proposal on

[*]giuseppe.burgio@uni-tuebingen.de
[†]markus.quandt@uni-tuebingen.de
[‡]hugo.reinhardt@uni-tuebingen.de
[§]hannes.vogt@uni-tuebingen.de

[1]The horizon condition selects among several possible solutions in the variational approach, while it comes out self-consistently in the renormalization group approach [14]. Physically, this can be interpreted as a vanishing dielectric constant of the vacuum, i.e., a manifestation of the dual Meissner effect [11].

the lattice and analyze its consequences on the correlators which should bear the signature of the Gribov-Zwanziger confinement mechanism. As a by-product, we also reanalyze the *bc* strategy with very high statistics, as finding a small eigenvalue of the Faddeev–Popov operator requires the analysis of a very large number of gauge copies.

II. THE GRIBOV PROBLEM

As Gribov has shown long ago [1], the Coulomb gauge condition $\partial_i A_i = 0$, among others, is not sufficient to select a single configuration from the gauge orbit uniquely. On the lattice, gauge fixing amounts to selecting, for each given configuration $\{U_\mu(x)\}$ of links, a gauge rotation $g(x) \in SU(N_c)$ such that some (unique) condition is met. In particular, Coulomb gauge fixing is achieved by maximizing, for each time slice t, the functional

$$F_t^U[g] = \frac{1}{N_c N_d V} \sum_{\mathbf{x},i} \mathrm{Retr}[U_i^g(t,\mathbf{x})], \tag{1}$$

where V is the spatial volume of the lattice and the sum extends over all spatial links only. A *local* maximum of (1) picks out—more or less randomly—one copy in the first Gribov region (where the Faddeev–Popov operator is positive definite), out of many others that all satisfy the same condition. A unique prescription, which would solve the Gribov problem completely, would amount to finding the *global* maximum, i.e., the representative of the gauge orbit in the so-called fundamental modular region (FMR). Finding such a global maximum of a function with many degrees of freedom is, however, analogous to finding the ground state of an $SU(N)$ spin glass [23], a problem which is known to be NP-hard even for the much simpler case of the $\mathbb{Z}_2$ gauge theory [24].

In the past, two approaches have been widely used to tackle the problem of Gribov copies in lattice gauge theory. The first one is to simply neglect that there is a problem at all, essentially stating that Gribov copies have no physical significance. In this case, the first (local) maximum found by the algorithm is selected and one proceeds in calculating all relevant (gauge dependent) quantities. In the literature, this process goes under the name of "minimal gauge" [25].[2]

The second approach is to choose the copy with the highest value of the gauge functional as the "best representative" of the global maximum, based on the conjecture that results for gauge-dependent quantities will be strongly correlated with the value of the gauge functional. In order to clarify this statement, let $\{U_{\mathrm{FMR}}\}$ be the ensemble of gauge configurations which are in the FMR, i.e., $F[U_{\mathrm{FMR}}] = \max$, and let $\{U_{bc}\}$ be the ensemble with gauge configurations close to such a maximum

$$F[U_{\mathrm{FMR}}] \gtrsim F[U_{bc}], \tag{2}$$

i.e., the set of configurations which correspond to the best maximum one could find numerically. The assumption is that the U_{bc} are, in some sense, "close" to the U_{FMR}, and this carries over to the expectation value of any gauge variant quantity Ω, i.e.,

$$\langle \Omega(U_{bc}) \rangle \approx \langle \Omega(U_{\mathrm{FMR}}) \rangle \equiv \langle \Omega \rangle_{\mathrm{phys}}. \tag{3}$$

No mathematical proof of this assumption exists, and a direct numerical test is only feasible for toy models on very small lattices. One such test, a U(1) lattice theory on a 2-dimensional sphere, actually provides numerical evidence *against* the hypothesis in Eq. (3) [28]. For historical reasons, we call the ensemble $\{U_{bc}\}$ the *best copy* (*bc*) ensemble.

A third approach for resolving the Gribov problem has been discussed for Landau gauge in Refs. [29,30]: instead of choosing the copy with the best value of the gauge functional, one picks the copy for which the first nontrivial eigenvalue of the Faddeev–Popov operator is smallest, the so-called *lowest copy* (*lc*). We borrow this notation from the aforementioned papers. The idea behind the *lc* approach is that this should choose configurations that are close to the Gribov horizon where the Faddeev–Popov operator becomes singular. According to Gribov's and Zwanziger's entropic reasoning, such configurations should be the relevant ones in the thermodynamic limit. The authors of Refs. [29,30] found that both the ghost dressing function and—to a much smaller extent—the gluon propagator are enhanced in the IR for the lowest-eigenvalue copy when compared to the *bc* approach, while they become flatter if one chooses a copy with a large eigenvalue of the Faddeev–Popov operator instead. Similar attempts to tweak the Landau gauge fixing procedure in order to make the IR behavior of the ghost propagator match the decoupling solutions found in the continuum (e.g., by Dyson–Schwinger or Functional Renormalization Group techniques) had previously been put forward with mixed results [31,32].

As discussed in the Introduction, a quantitative discrepancy exists in the Coulomb gauge between the IR exponent of the ghost dressing function in the Hamiltonian variational approach [8–10,13] and the corresponding lattice results [19–21]. On the other hand, the behavior of the gluon propagator agrees very well between the two approaches [15,16]. Since the IR exponents of the ghost form factor and the gluon propagator should be related by a sum rule which is based on the sole assumption that the ghost-gluon vertex should be bare, or at least nonsingular, in the deep infrared [10] (a fact that is known to hold in

[2]In the literature the term *minimal gauge* had originally been applied in Landau gauge to the representative of the fundamental modular region along the gauge orbit [26,27]. Later, the term *absolute gauge* stuck for this case, while minimal gauge was "downgraded" to its present use [25].

Landau gauge and expected to carry over to Coulomb gauge[3]), this poses an unresolved puzzle.

One possible explanation for such disagreement is that the variational approach would have to be improved in order to better reproduce the lattice results. This goes beyond a mere improvement of the variational *ansatz*, since the sum rule must hold for any *ansatz* (assuming a nonsingular ghost-gluon vertex in the IR). One possible idea is that the proper implementation of the GZ idea would go beyond the standard Coulomb Hamiltonian combined with the horizon condition, and additional terms in the action or Hamiltonian would be required, which could eventually reconcile the sum rule with lattice propagators. There are some indications that such a refinement is necessary in Landau gauge, where additional condensates can be introduced in the GZ action in order to make the GZ scenario agree with lattice data [36]. In the Hamiltonian approach, however, we see no compelling evidence for such a modification, in particular, since the present investigation will show that there is no such thing as "the lattice propagators" in Coulomb gauge, at least with current computational power. It would then be very hard to identify the proper extension of the Coulomb gauge GZ scenario required to match the inconsistent lattice data.

This leaves us with the second logical explanation for the sum-rule puzzle, namely, that the current lattice simulations in Coulomb gauge do not describe continuum physics and hence need refinement. More precisely, the *bc* strategy on the lattice could be biased by artifacts related to the Gribov problem, being unable to come close enough to the Gribov horizon, and the *lc* strategy might provide a better description of continuum physics [22]. To check this conjecture we adapt in the following the *lc* strategy to Coulomb gauge.

III. LATTICE SETUP

For our study, we use the colour group $G = SU(2)$ for simplicity and employ the isotropic and the anisotropic Wilson gauge action [37]

$$S = \sum_x \left\{ \beta_s \sum_{j>i=1}^{3} \left(1 - \frac{1}{2}\mathrm{Retr} U_{ij}(x)\right) + \beta_t \sum_{i=1}^{3} \left(1 - \frac{1}{2}\mathrm{Retr} U_{i4}(x)\right)\right\}, \quad (4)$$

where we parametrize $\beta_s = \beta\gamma$ and $\beta_t = \beta/\gamma$, with γ the bare anisotropy, while $\xi = a_s/a_t$ denotes the renormalized anisotropy in the following. We have used isotropic lattices of three different sizes and discretizations in our analysis. Since the ghost propagator is known to suffer from strong scaling violations on isotropic lattices, we include two anisotropic lattices of fixed size. Our setup is summarized in Table I. To fix the lattice spacing, we used the $SU(2)$ results known from the literature as summarized in the tables given in Ref. [15]. We have also fixed $\sqrt{\sigma} = 0.44$ GeV to set the physical scale.

TABLE I. Lattice setup.

Label	Size	ξ	β	a_s [GeV^{-1}]	L [fm]
A1	16^4	1	2.2	1.07	3.4
A2	16^4	1	2.3	0.84	2.6
A3	16^4	1	2.4	0.61	1.9
B1	24^4	1	2.2	1.07	5.0
B2	24^4	1	2.3	0.84	4.0
B3	24^4	1	2.4	0.61	2.9
C1	32^4	1	2.2	1.07	6.7
C2	32^4	1	2.3	0.84	5.3
C3	32^4	1	2.4	0.61	3.8
D1	128×32^3	4	2.25	1.11	7.0

IV. GAUGE FIXING AND GRIBOV COPIES

Both for the *lc* and the *bc* strategy, we use the over-relaxation technique [38] in the CUDA implementation cuLGT [39]. In Ref. [39], simulated annealing [40,41] is also discussed as a technique to increase the probability to find the absolute maximum of the gauge fixing (g.f.) functional, i.e., to find a better best-functional copy. By now, the *de facto* standard technique to find the (best approximation of the) global maximum is a combination of repeated gauge fixing and a preconditioning with simulated annealing [42,43]. In this context, repeated gauge fixing means to start the gauge fixing multiple times from a random gauge transformation and select the copy which best satisfies the *bc* (or *lc*) condition. In Fig. 1, we show an illustrative plot of the evolution of the gauge fixing precision

$$\theta \equiv \frac{1}{N_c} \max_{\mathbf{x}} \mathrm{tr}[\Delta(x)\Delta^\dagger(x)] \quad (5)$$

with

$$\Delta(x) \equiv [\partial_i A_i]^{\mathrm{lat}} = \sum_i [A_i^{\mathrm{lat}}(x) - A_i^{\mathrm{lat}}(x-\hat{\imath})]$$

over the number of gauge fixing steps. In the figure on the left-hand side, four runs with the over-relaxation parameter $\omega = 1.7$ and one run with $\omega = 1$ (pure relaxation) are shown. The gauge fixing has two characteristic stages: In the first stage the precision is fluctuating strongly at a rather high value until a maximum is located with a precision of

[3]In Landau gauge, the vertex is expected to be unrenormalized based on Slavnov-Taylor identities [33]; this is confirmed by lattice simulations which find only mild deviations from a bare vertex over the entire momentum range [34]. A similar conclusion can also be made in Coulomb gauge within the variational approach (using the continuum propagators as input) [35].

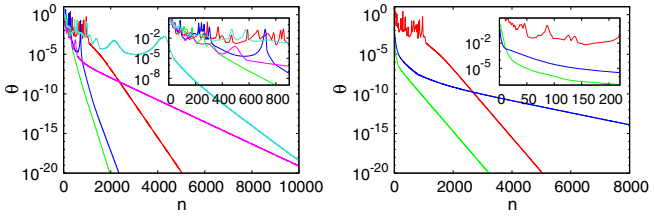

FIG. 1. Gauge precision θ over the number of over-relaxation steps. Left panel: Five gauge copies of the same configuration. The light blue (top) curve is with simple relaxation; the other lines correspond to over-relaxation ($\omega = 1.7$). The pink line with the smallest slope corresponds to a significantly smaller value (compared to the other copies) of the first nontrivial eigenvalue λ_1 of the FP operator. Right panel: Red (top) and green (bottom) line correspond to over-relaxation ($\omega = 1.7$) without (red) and with (green) simulated annealing preconditioning. As can be seen, the preconditioning removes the first phase where the algorithm tries to locate a maximum, while the slope of the second phase (the eventual convergence speed) is unchanged. The blue curve in the middle employs preconditioning with simple relaxation ($\omega = 1$) and shows no fluctuating first phase but a much smaller convergence speed. All three lines converge towards the same Gribov copy, as was confirmed by identical functional values and an identical first nontrivial FP eigenvalue.

about $\theta \approx 10^{-4}$. Then, in the second stage, the precision monotonically approaches zero. As shown on the right-hand side, if simulated annealing preconditioning is used, the first stage is already overcome in the simulated annealing phase (which is not shown in the plot).

As we focus on the *lc* approach in this study, our goal is not to bias our algorithm towards copies with a high value of the g.f. functional, and we thus have to waive the simulated annealing preconditioning. Since the *bc* results in this chapter are mostly obtained as a by-product of the main search for the lowest-eigenvalue copy, they are also not preconditioned with simulated annealing, unless explicitly stated otherwise. Unfortunately, no algorithm is known that would precondition the gauge fixing to a low eigenvalue of the Faddeev–Popov operator, and we have to rely on pure over-relaxation with a high number of gauge copies N_r.

In a first run, we calculated the lowest eigenvalue λ_1 on $N_r = \mathcal{O}(10^3)$ copies of the small lattices. In Ref. [44], it was noticed that the size of the smallest eigenvalue is correlated with the number of gauge fixing iterations N_{it} that are necessary to achieve a given accuracy θ, as indicated in Fig. 1. The reason for this behavior is that a low eigenvalue means an almost flat direction in the g.f. functional and an ill-conditioned Faddeev–Popov operator, leading to a slow convergence of the iteration process. In Fig. 2, we investigated this behavior in more detail. We find a perfect correlation of λ_1 and N_{it}, independently of the coupling β, with the slope only depending very weakly on the over-relaxation parameter ω. In fact, we find that all data can be perfectly described by the simple power law

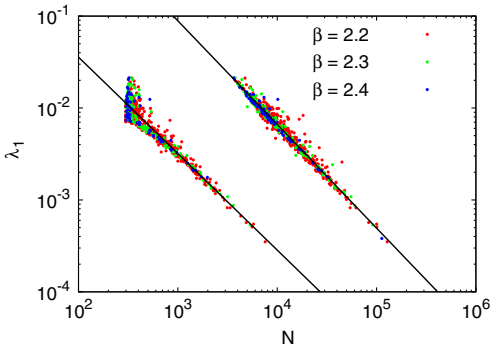

FIG. 2. Smallest eigenvalue λ_1 of the Faddeev–Popov operator as a function of the number of gauge-fixing iterations. From each set A1, A2, and A3, we used 10 configurations and calculated 1000 gauge copies. The data points which correspond to fewer iterations (left) are from runs with $\omega = 1.9$; for the points with more iterations (right), we used $\omega = 1$.

$$\lambda_1(N_{\mathrm{it}}) = \frac{c}{N_{\mathrm{it}}^{\gamma}}, \tag{6}$$

with $\gamma \approx 1.1$ and the proportionality factor c strongly depending on ω. To rule out that the over-relaxation parameter ω conditions the algorithm to find a gauge copy with specific value of λ_1, we verified that ω has no influence, on average, on how often a configuration with small eigenvalue is found. This is also indicated in Fig. 2, though in the plot it is obfuscated by the bulk around the minimal number of iterations.

The correlation of the number of iterations and the smallness of the Faddeev–Popov eigenvalue allow us to tweak our algorithm: Since the calculation of eigenvalues is computationally the most demanding part in our gauge fixing program, we implemented a (self-adjusting) threshold, where the eigenvalues are calculated only for "promising" gauge copies for which the number of iterations exceeds a certain value. Since the smallest eigenvalue (which we are able to find) differs from configuration to configuration, we usually re-start with a small threshold for each configuration. If we do find a small eigenvalue, the threshold is updated to a factor α of the number of iterations that were needed to find this particular (small) eigenvalue. We find that $\alpha = 0.8$ provides a suitable update strategy: With this setting eigenvalues are calculated in a typical run for many gauge copies up to a point where a small eigenvalue is found and the threshold is changed. Since usually the Gribov copies with the smallest eigenvalue are well separated from the one with the next-to-smallest eigenvalue, this procedure constrains the program to only evaluate the eigenvalues for promising configurations with the smallest λ_1.

Since the first Gribov region and the FMR have a common boundary, one may wonder if the *bc* approach, which can be seen as an approximated search for configurations in the FMR, and the *lc* approach, as an

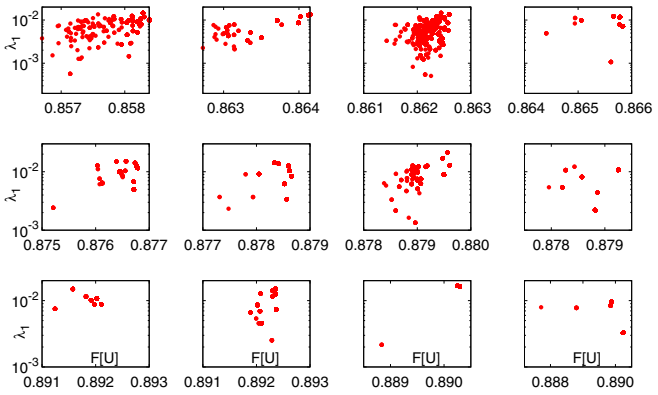

FIG. 3. Smallest eigenvalue vs functional value for 1000 copies from four arbitrary configurations of the 16^4 lattices A1, A2, A3 (from top to bottom). The number of distinct Gribov copies decreases with finer lattices.

approximated search for configurations close to the Gribov horizon, eventually converge to the same configuration. However, from the Landau gauge data [29], there is no such indication. Also for our Coulomb gauge data, there is no evidence that the *bc* and *lc* procedures may coincide. In Fig. 3, we show scatter plots for four arbitrarily selected configurations of each of the small (16^4) lattices A1, A2, and A3 from top to bottom. The data points are from 1000 different gauge copies, but there are many fewer points as the same Gribov copy is often found multiple times. In fact, the number of distinct Gribov copies varies strongly between configurations, compare, for instance, the third and fourth configuration of the A1 lattice (top right). As expected, the number of distinct Gribov copies decreases with finer lattice spacing.

Another indication that *bc* and *lc* are different gauges is the result of Fig. 4. There, we compare the best approximation of the FMR and the Gribov horizon for all 100 configurations of the 24^4 sets B1 and B3 after 1000 and 10,000 gauge copies, respectively. Neither on the coarse lattice (B1) nor on the fine lattice (B3) could we find any

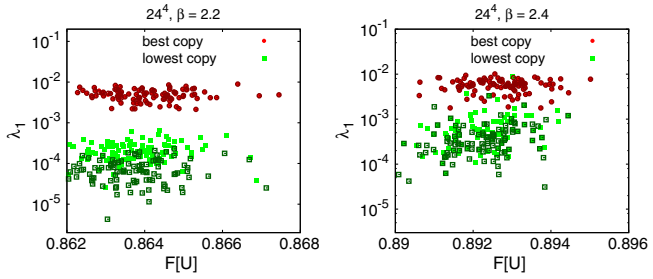

FIG. 4. Best approximation of the FMR, i.e., the b -approach, and the Gribov horizon, i.e., the *lc* approach. Full light-colored symbols denote 1000 trials; the empty, dark-colored symbols denote 10,000 gauge copies. Lattices: B1 (left), B3 (right). There is no configuration where $bc = lc$.

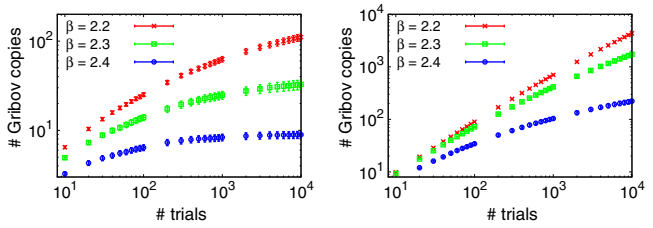

FIG. 5. Number of distinct Gribov copies vs the number of gauge copies for the 16^4 (left) and the 24^4 (right) lattices. Only for the fines 16^4 lattice a saturation is observed. The Gribov copy is identified only by the value of the gauge fixing functional.

configuration where the best functional and the lowest-eigenvalue copy coincide. For the coarse lattice with 10,000 copies, the smallest eigenvalues are well separated, by at least an order of magnitude, in a first region with all the *bc* copies and a second region with the *lc* copies. While only very few (B1) or no configurations (B3) see a decrease of the lowest eigenvalue λ_1, in the *bc* case, as we go from 1000 to 10,000 copies, the *lc* data still sees a considerable reduction of λ_1. A similar comparison was made for Landau gauge in Ref. [32]. There, the authors used the value of the ghost propagator at the smallest nonzero momentum as an estimate of the smallness of the lowest FP eigenvalue. While they used a much larger ensemble of $\approx\mathcal{O}(10^3)$ configurations, they used much less gauge fixing repetitions $\approx\mathcal{O}(10)$. With this setup, they found configurations that are close to *both* the FMR and the Gribov horizon. However, it is clear that their setup (many configurations, small N_r) is specifically biased towards finding such configurations, while our setup is biased in the opposite direction (fewer configurations, large N_r). For a detailed study of this effect, which is not our focus, we would have to significantly increase the statistics.

Finally, we try to estimate the number of Gribov copies in Fig. 5 by counting how many distinct Gribov copies we are able to find for a given number of g.f. attempts. For this study, we use only the functional value to identify the Gribov copy, since we do not have the smallest eigenvalue available for all copies (due to the threshold strategy described above). In general, an unambiguous identification of a Gribov copy would require identical values for *all* gauge-dependent quantities; the use of only a single quantity (the g.f. functional) may therefore erroneously take distinct copies as identical, i.e., the procedure is biased towards finding too many identical and too few distinct copies.[4] An unambiguous estimate would furthermore require that each Gribov copy is found with equal probability; however, very likely there are local maxima which are easier to locate by the algorithm. This effect will lead to

[4]Additionally, the authors of Ref. [32] found that there are gauge copies with the same functional value but a different value for the ghost propagator at smallest nonzero momentum.

an underestimation of the number of distinct Gribov copies. Thus, the result in Fig. 5 has to be treated very carefully. More comprehensive studies of the number of Gribov copies in lattice gauge theory can be found, for example, in Refs. [45,46].

Since the number of Gribov copies varies considerably between different configurations, the error bars are rather large. Only on the smallest and finest lattice a saturation of the number of Gribov copies is observed within 10,000 g.f. attempts. The main conclusion we can draw from Fig. 5 is that we are far from having explored the whole Gribov region, which would be essential if the absolute lowest-eigenvalue copy still differs substantially from the lowest-eigenvalue copy in our limited search space.

V. RESULTS

While there is no compelling reason for the *lc* approach to have a large effect on the gluon propagator, we expect a clear impact on the ghost propagator, given its spectral representation

$$G(\mathbf{p}) = \sum_n \frac{\phi_n(\mathbf{p})\phi_n(-\mathbf{p})}{\lambda_n}, \tag{7}$$

where λ_n are the eigenvalues and $\phi_n(\mathbf{p})$ the momentum space eigenfunctions of the Faddeev–Popov operator. As for the Coulomb potential, one also expects a large effect from the *lc* strategy. Let us discuss them case by case.

A. Gluon propagator

In Landau gauge, a small Gribov copy dependence was observed for the gluon propagator on a large 54^4 lattice in the deep IR [29]. With our lattice setup, we are not able to reach that far in the IR and do not see a significant effect on the Coulomb gauge gluon propagator $D(\mathbf{p})$ as defined in Refs. [15,16]; see Fig. 6, where we plot $D(\mathbf{p})/|\mathbf{p}|$ to underline its IR behavior.[5] Since the accurate calculation of $D(\mathbf{p})$ requires the technique illustrated in Refs. [15,16], the Coulomb gauge needs to be fixed for *all* time slices. This limits the number of g.f. repetitions as compared to the study of the Faddeev–Popov-operator-dependent quantities in the following sections, which can all be evaluated on a single time slice.

B. Ghost propagator

As expected from Eq. (7), the Gribov copy effect (i.e., the different g.f. prescriptions of picking Gribov copies) has a huge impact on the ghost propagator as defined in Refs. [19]. In Fig. 7, we see that for the 24^4 lattice the ghost form factor is drastically enhanced in the IR as the number of repetitions of the *lc* strategy increases.

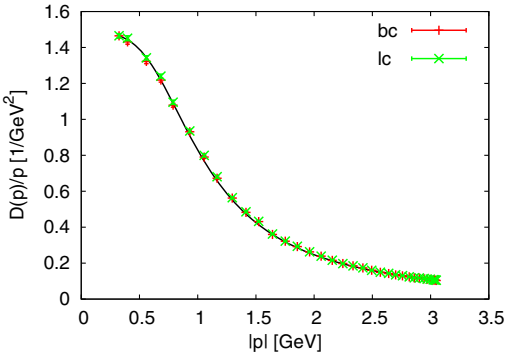

FIG. 6. The gluon propagator for the B1 lattice with the *bc* and *lc* approaches from 1000 trials. The solid line is a fit to the Gribov formula [15,16]. The choice of Gribov copy apparently makes no visible difference.

For both the coarse and the fine lattice, the effect first becomes visible upon reaching about 100 repetitions. From this point on, the form factor is clearly increased when going from 100 to 1000 copies, while the further increase between 1000 and 10,000 copies is less pronounced. This may be taken as a hint towards an eventual convergence, although no saturation of the effect can be really observed within our available data. The huge difference in the IR is mainly due to a sharper bending in the region between 1 and 3 GeV.

It should be noted that the data for different β have been presented in different plots on purpose: The ghost form factor is known to suffer from scaling violations on isotropic lattices [19], so that data points for different β do not fall on top of each other over the whole momentum range (after multiplicative renormalization). Moreover, since the curves in the *lc* approach curves have not yet converged, the data from different β cannot be compared, as the quality of the *lc* gauge fixing for given N_r most likely depends on the coupling β.

In Fig. 8, we compare the ghost form factor within the *bc* approach for the same lattices. First of all, the effect of taking more g.f. repetitions is much less pronounced as

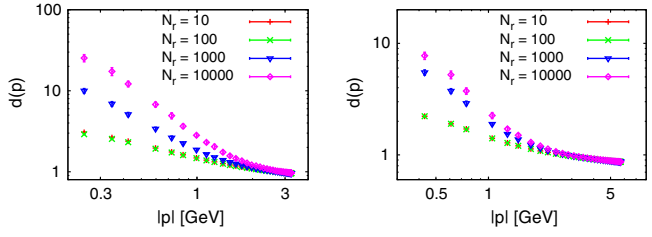

FIG. 7. The ghost form factor after gauge fixing to the lowest-eigenvalue copy with increasing number of trials from 10 to 10,000 on 24^4 lattices at $\beta = 2.2$ (B1, l.h.s.) and $\beta = 2.4$ (B3, r.h.s.).

[5]The expert reader will notice a strong similarity between the IR behavior of the gluon (and to a lesser extent ghost) propagators in the Coulomb and Landau gauge. This has been extensively discussed in Ref. [16,19] and can be simply ascribed to the presence of common IR (Gribov) mass scale in both cases.

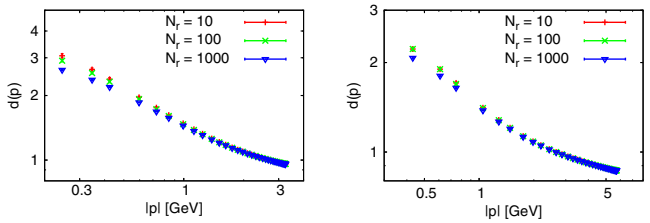

FIG. 8. The ghost form factor after gauge fixing to the best functional copy with increasing number of trials from 10 to 1000 on 24^4 lattices at $\beta = 2.2$ (B1, lhs) and $\beta = 2.4$ (B3, rhs). The data points for 10,000 copies are omitted since no better copy is found, compare Fig. 4.

compared to the *lc* approach results in Fig. 7. Secondly, the effect goes in the opposite direction: While the ghost form factor for the *lc* approach was enhanced in the IR, the IR form factor in the *bc* approach becomes slightly suppressed as the number of g.f. attempts is increased. The (small) effect is negligible between 10 and 100 repetitions, but becomes somewhat more pronounced in the region between 100 and 1000 repetitions. In Fig. 9, we compare the results for the *lc* and *bc* approaches with 10,000 copies, our best values at this lattice size, where we have renormalized the form factor to

$$d(p = 3\ \mathrm{GeV}) = 1. \tag{8}$$

The *bc* approach data at different β fit quite well on top of each other, especially when considering the scaling violations [19]. Compared to the *lc* strategy, the error bars for the *bc* strategy are much smaller.

To extract the IR exponent of $d(p)$, we have fitted the data at different N_r for the D1 ensembles in Table I. Since their UV tail is not extended enough to extract reliably any UV logarithmic exponent, we used the simplest function interpolating between a power law in the IR and a constant in the UV:

$$d(p) = p^{-\kappa}\frac{P_{n-1}(p) + a p^{n+\kappa}}{R_{n-1}(p) + p^n}, \tag{9}$$

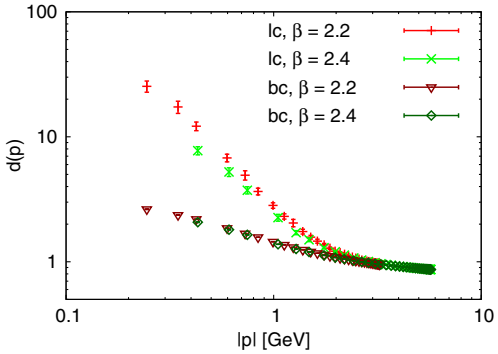

FIG. 9. The ghost form factor from the lattices B1 and B3 after 10,000 copies of *bc* and *lc* strategies.

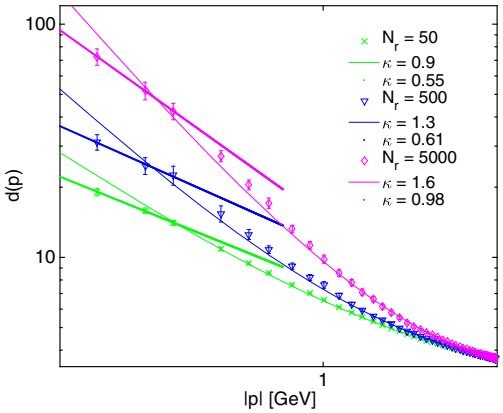

FIG. 10. Fits of $d(p)$ to an IR power law for the D1 lattices. The continuous lines are the fits to Eq. (9); the dotted lines just fit the last three points to a power law. The respective κ values are given in the legend.

where P_{n-1} and R_{n-1} are polynomials of degree $n-1$ and the denominator is constrained not to have any real poles (see, e.g., Ref [19]). Here, $n = 2$ gives already a good enough fit, and the results are given in Fig. 10 (continuous lines). While in the *bc* strategy we consistently found $\kappa \simeq 0.5$ (see Refs. [19–21]), for the *lc* strategy the exponent reaches $\kappa \simeq 0.9$ already for $N_r = 50$ and keeps on growing as N_r increases, reaching $\kappa \simeq 1.6$ for $N_r = 5000$, with no apparent saturation; the values of χ^2/DOF range between 0.9 and 1.4. The fits seem however to miss the underlying behavior in the lowest IR region. Indeed, the good χ^2/DOF values come from the $p > 1$ GeV data, while below these the curves clearly overestimate the IR behavior; changing n does not improve the situation. We have also tried to directly fit the last points to a power law, neglecting any subleading behavior: $d(p) = A p^{-\kappa}$. The results are also shown in Fig. 10. Although for $N_r = 5000$ we obtain for κ a value close to the continuum predictions, the evident lack of saturation still means that by increasing N_r we would probably overshoot $\kappa = 1$ again. Moreover, the low momentum data are known to be effected by large IR cutoff effects: Only simulations at higher volumes could eventually deliver reliable results.

All in all, the lack of saturation in the data will pose a challenge to any fitting strategy, even if a theoretically sound *Ansatz* for $d(p)$ over the whole momentum range, going beyond a simple power law, could be found. We will see in the next section that such lack of saturation is an even bigger problem for the calculation of the Coulomb potential.

C. Coulomb potential

The most important quantity for Coulomb gauge confinement is the Coulomb potential, since it provides direct access to the Coulomb string tension; this quantity can be computed from the momentum space Coulomb kernel [19]:

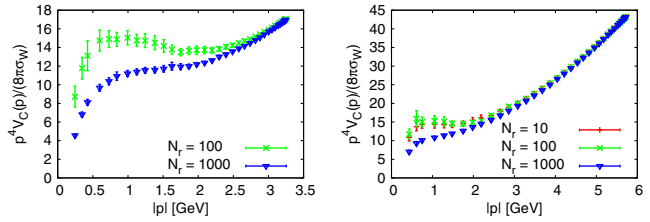

FIG. 11. Coulomb potential in the *bc* approach as a function of N_r. The data with $N_r = 10,000$ are omitted, since they show no difference as compared to $N_r = 1,000$, see Fig. 4.

$$V_C(\mathbf{p}) = g^2 \mathrm{tr}\langle(-\hat{\mathbf{D}}\cdot\nabla)^{-1}(-\nabla^2)(-\hat{\mathbf{D}}\cdot\nabla)^{-1}\rangle. \quad (10)$$

A linearly rising potential for large distances corresponds to a momentum space potential diverging like $1/p^4$ in the IR. Thus, it is convenient to plot the potential such that its intercept with the y-axis yields the Coulomb string tension σ_C in units of the physical (Wilson) string tension σ,

$$\frac{p^4 V_C(p)}{8\pi\sigma} \xrightarrow{p\to 0} \frac{\sigma_C}{\sigma}. \quad (11)$$

In Fig. 11, the ratio Eq. (11) is shown, within the *bc* approach, for the same configurations used in Fig. 8 for the ghost propagator.[6] In earlier studies of the Coulomb potential, a bump in $p^4V_C(p)$ was observed at around 0.5 to 1 GeV, affecting direct estimates of the intercept on the vertical axis with large uncertainties [19–21,47–49]. As Fig. 11 shows, this bump does indeed vanish as the number of gauge copies is increased; at the same time, the statistical precision on the MC data strongly improve. One might be tempted to assume that one is actually approaching the absolute maximum of the gauge-fixing functional as the number of gauge copies is increased and the ensemble eventually samples a FMR free of Gribov copies.[7] If this was the case, however, one should expect that the Coulomb potential from the alternative *lc* approach should yield the same (or a similar) result, as the Gribov-Zwanziger entropic argument in the thermodynamic limit states that the partition function is dominated by configurations lying on the common boundary of the FMR and the first Gribov region. For such configurations, the *bc* and *lc* approaches—once they converged—would give identical results.

Unfortunately, the *lc* result for the Coulomb potential does not corroborate such a conjecture. In Fig. 12, the data for the *bc* and the *lc* approaches are compared for the B1 and B3 lattices. While for the ghost propagator, the different gauge fixing strategies provided a nice overlap in

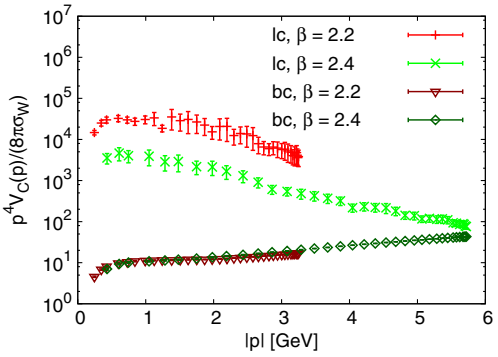

FIG. 12. The Coulomb potential from the lattices B1 and B3 after 10,000 copies.

the UV regime (see Fig. 9), the Coulomb potential, over the whole momentum range, is increased by *several orders of magnitude*. The same happens for all lattices that we investigated. Since this result is quite surprising, we have repeated the calculation with a different solver. We have usually adopted a conjugate gradient algorithm with Laplace preconditioning. To ensure the validity of our solver for exceptional configurations[8] we compared the results of our conjugate gradient to a publicly available C++ implementation [51] of the MINRES algorithm [52]. Both algorithms yield the same solution up to numerical precision.

Interestingly, while the Coulomb potential in the *lc* approach computed from the kernel Eq. (10) apparently yields physically nonsensible results, the alternative definition proposed in Refs. [53,54], which is based on short Polyakov lines P_t of length t and the correlator of temporal links U_0,

$$\begin{aligned} aV_C(|\mathbf{x}-\mathbf{y}|) &= -\lim_{t\to 0}\frac{d}{dt}\log\langle \mathrm{tr}P_t(\mathbf{x})P_t^\dagger(\mathbf{y})\rangle \\ &= -\log\langle \mathrm{tr}U_0(\mathbf{x})U_0^\dagger(\mathbf{y})\rangle, \end{aligned} \quad (12)$$

seems to work in all cases, cf. Fig. 13. As in the case of the gluon propagator, the effect of choosing different g.f. strategies and selection of Gribov copies is quite modest. To extract the Coulomb string tension, we fitted V_C from Eq. (12) to

$$V_C(r) = \frac{\alpha}{r} + \sigma_C r + \mathrm{const}, \quad (13)$$

where the Lüscher term $\alpha = -\frac{\pi}{12}$ is kept fixed. In the range $[6/a, 14/a]$, we find a Coulomb string tension varying

[6]In the $\beta = 2.2$ plot on the left-hand side, the data for $N_r = 10$ is omitted, since it contained a configuration with a small eigenvalue leading to very big error bars. We discuss the issue in more detail below.

[7]We had put forward such hypothesis in Ref. [50], although in a slightly different context.

[8]The *lc* strategy generally attempts to make the Faddeev–Popovoperator ill conditioned. But for some configurations with a very small eigenvalue λ_1, it becomes nearly singular, and its precise inversion in the Coulomb potential is numerically challenging.

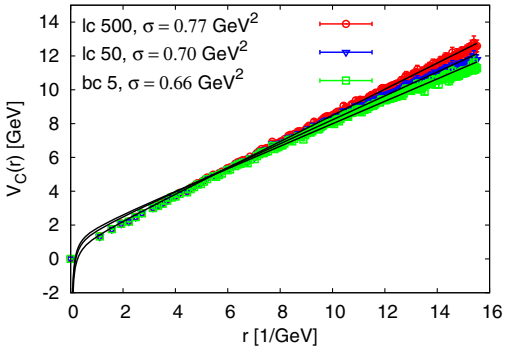

FIG. 13. Coulomb potential in position space from the $\langle U_0 U_0^\dagger \rangle$ correlator in Eq. (12) (D1 lattice). The *bc* configurations are preconditioned with simulated annealing.

between $(0.66\ \mathrm{GeV})^2$ (*bc* 5) and $(0.77\ \mathrm{GeV})^2$ (*lc* 500), with χ^2/DOF between 0.58 (*lc* 500) and 0.95 (*bc* 5).

VI. CONCLUSIONS

In this paper, we have studied the effect of fixing, on the lattice, the Coulomb gauge to the copy closest to the Gibov horizon, i.e., the copy with the smallest nonvanishing eigenvalue of the Faddeev–Popov operator (*lc approach*). This prescription *de facto* implements the proposal of Ref. [22]. The main observation we made is that the size of the smallest eigenvalue saturates very slowly, if at all, with the number of gauge-fixing attempts, see, e.g., Fig. 4. Of course, we are still far from exploring the whole Gribov region, as Fig. 5 suggests; still, our result is somehow surprising. In light of the entropic argument usually made within the Gribov-Zwanzier scenario, one would have intuitively expected that the small eigenvalue of the Faddeev–Popov operator should be bounded from below by some effective IR cutoff induced by the finite lattice volume; we however see no such saturation even after $N_r = 10,000$ gauge-fixing repetitions.

The small eigenvalues heavily affect the IR behavior of the ghost propagator and, more importantly, the Coulomb potential extracted from the kernel in Eq. (10). The first effect can be regarded as positive to some extent, as it moves the infrared behavior of the ghost propagator towards the continuum prediction and thus reduces the violation of the sum rule. As with the size of the smallest eigenvalue, we do not see a saturation with the number of gauge copies, and the ghost exponent eventually tends to overshoot the continuum prediction. However, given the arbitrariness in the fits used to extract the exponent, it is at least conceivable that the *lc approach* could indeed be made to agree with the continuum.

Much more severe is the second effect, on the Coulomb potential, which yields results that are at odds with physical expectations. The dramatic increase of the potential extends the entire momentum range and also affects the Coulomb string tension, to the point that the results are physically nonsensible. As the effect on the eigenvalues has not yet saturated with $N_r = 10,000$ gauge-fixing repetitions, exploring the Gribov region further by increasing N_r should make things even worse.

We can think of several possible interpretations of our result. First, it could be that merely constraining the lowest eigenvalue is insufficient to detect the physical relevant configurations. From the entropic argument, one expects the partition function to be peaked on the common boundaries of the first Gribov region and the fundamental modular region, i.e., on configurations where the absolute maxima of Eq. (1) become degenerate. The multiple flat directions allow for further refinements of the *lc* prescription; for instance, a restriction to configurations where *at least* the two lowest eigenvalues are small *and* (nearly) degenerate could lead to the correct physics. Such an investigation is, although numerically demanding, in principle, feasible, and its implementation is currently under scrutiny.

A second possibility is that the Coulomb potential as calculated from Eq. (10) involves the inverse of the ill-conditioned lattice Faddeev–Popov operator whose kernel may be sensitive to the exact lattice definition and (yet to be determined) discretization artifacts. The *lc* procedure would then bring this defect to the fore and amplify it, ultimately making the lattice definition impractical. The fact that the alternative definition given in Eq. (12), which requires no such operator inversion, always works well might indeed point in this direction. Also, the fact that no saturation for the smallest eigenvalue could be found hints towards spurious artifacts in the low-lying spectrum of the lattice Faddeev–Popov operator. If this issue could be resolved and a saturation could be found, it is also conceivable that a theoretically motivated *Ansatz* for the fit to the data in Fig. 10 might still bring the results in agreement with the continuum predictions, e.g., the ghost exponent $\kappa = 1$.

Alternatively one could argue that, since the fundamental discretization of Yang-Mills theory is known to possess lattice artifacts which affect gauge invariant, topological observables [55–58], it is conceivable for them to also influence gauge-dependent quantities. In this case, it is the discretization of the model itself which would introduce spurious quasi-zero modes in the FP operator which subsequently affect all quantities that require its inversion (such as the ghost propagator or the Coulomb potential). By contrast, ordinary correlators that require no FP inversion are benign, cf. Eq. (12). To test such a hypothesis one would, however, need to explore the Coulomb gauge in algorithmically demanding alternative discretizations of the Yang-Mills action [56,57,59,60].

Finally, it is also conceivable that the GZ scenario realized in the Hamiltonian approach does not describe the lattice results at all, and a refinement of the Coulomb Hamiltonian would be necessary, similarly to what was conjectured in Landau gauge [36]. If such a refinement is to

remain renormalizable, however, the additional terms would dominantly affect the infrared regime and, hence the sum rule, but they could not explain the dramatic increase of the Coulomb potential observed in the *lc* approach over the *entire* momentum range. More generally, the numerical investigations in this paper show that there is not one single consistent version of Coulomb gauge on the lattice, at least not within current computational limits, and it is hence unclear in which way to extend the continuum GZ scenario. At the moment, we have no strong evidence for an extension of the present continuum formulation, i.e., the standard Hamiltonian approach realizing the GZ horizon condition remains our best continuum description so far.

A by-product of our investigation was the systematic improvement of the search for the best gauge functional value (*bc* approach) with a high number of g.f. repetitions. While in this case gluon and ghost propagators (Figs. 6 and 8) do not change as compared to previous investigations [15,16,18–21], the Coulomb potential loses the "bump" in the low momentum region found in previous works, which allows for a much more reliable estimate of the Coulomb string tension in this setup. For a true high-precision determination of σ_C, however, larger volumes and a systematical finite size analysis would be required.

ACKNOWLEDGMENTS

This work was partially supported by the Deutsche Forschungsgemeinschaft under Contract No. DFG-Re 856/10-1. H. V. wishes to thank the Evangelisches Studienwerk Villigst for financial support.

[1] V. N. Gribov, Nucl. Phys. **B139**, 1 (1978).
[2] R. Jackiw, I. Muzinich, and C. Rebbi, Phys. Rev. D **17**, 1576 (1978).
[3] N. H. Christ and T. D. Lee, Phys. Rev. D **22**, 939 (1980).
[4] D. Schutte, Phys. Rev. D **31**, 810 (1985).
[5] D. Zwanziger, Phys. Rev. Lett. **90**, 102001 (2003).
[6] H. Reinhardt, M. Quandt, and G. Burgio, Phys. Rev. D **85**, 025001 (2012).
[7] A. P. Szczepaniak and E. S. Swanson, Phys. Rev. D **65**, 025012 (2001).
[8] C. Feuchter and H. Reinhardt, Phys. Rev. D **70**, 105021 (2004).
[9] H. Reinhardt and C. Feuchter, Phys. Rev. D **71**, 105002 (2005).
[10] W. Schleifenbaum, M. Leder, and H. Reinhardt, Phys. Rev. D **73**, 125019 (2006).
[11] H. Reinhardt, Phys. Rev. Lett. **101**, 061602 (2008).
[12] K. G. Wilson, Phys. Rev. D **10**, 2445 (1974).
[13] D. Epple, H. Reinhardt, and W. Schleifenbaum, Phys. Rev. D **75**, 045011 (2007).
[14] M. Leder, J. M. Pawlowski, H. Reinhardt, and A. Weber, Phys. Rev. D **83**, 025010 (2011).
[15] G. Burgio, M. Quandt, and H. Reinhardt, Phys. Rev. Lett. **102**, 032002 (2009).
[16] G. Burgio, M. Quandt, and H. Reinhardt, Phys. Rev. D **81**, 074502 (2010).
[17] M. Quandt, H. Reinhardt, and G. Burgio, Phys. Rev. D **81**, 065016 (2010).
[18] G. Burgio, M. Schröck, H. Reinhardt, and M. Quandt, Phys. Rev. D **86**, 014506 (2012).
[19] G. Burgio, M. Quandt, and H. Reinhardt, Phys. Rev. D **86**, 045029 (2012).
[20] G. Burgio, M. Quandt, H. Reinhardt, M. Schröck, and H., Vogt, *Proc. Sci.*, LATTICE20132014 (2014) 365.
[21] G. Burgio, M. Quandt, H. Reinhardt, and H. Vogt, Phys. Rev. D **92**, 034518 (2015).
[22] P. Cooper and D. Zwanziger, Phys. Rev. D **93**, 105024 (2016).
[23] E. Marinari, C. Parrinello, and R. Ricci, Nucl. Phys. **B362**, 487 (1991).
[24] F. Barahona, J. Phys. A **15**, 3241 (1982).
[25] A. Maas, Phys. Rev. D **79**, 014505 (2009).
[26] A. Cucchieri, Nucl. Phys. **B508**, 353 (1997).
[27] A. Cucchieri, Nucl. Phys. **B521**, 365 (1998).
[28] P. de Forcrand and J. E. Hetrick, Nucl. Phys. B, Proc. Suppl. **42**, 861 (1995).
[29] A. Sternbeck and M. Müller-Preussker, Phys. Lett. B **726**, 396 (2013).
[30] A. Sternbeck and M. Müller-Preussker, *Proc. Sci.*, ConfinementX (2012) 074.
[31] A. Maas, Phys. Lett. B **689**, 107 (2010).
[32] A. Maas, Phys. Rev. D **93**, 054504 (2016).
[33] J. C. Taylor, Nucl. Phys. **B33**, 436 (1971).
[34] A. Cucchieri, A. Maas, and T. Mendes, Phys. Rev. D **77**, 094510 (2008).
[35] M. Q. Huber, D. R. Campagnari, and H. Reinhardt, Phys. Rev. D **91**, 025014 (2015).
[36] A. Cucchieri, D. Dudal, T. Mendes, and N. Vandersickel, Phys. Rev. D **85**, 094513 (2012).
[37] G. Burgio, A. Feo, M. J. Peardon, and S. M. Ryan (TrinLat), Phys. Rev. D **67**, 114502 (2003).
[38] J. E. Mandula and M. Ogilvie, Phys. Lett. B **248**, 156 (1990).
[39] M. Schröck and H. Vogt, Comput. Phys. Commun. **184**, 1907 (2013).
[40] S. Kirkpatrick, C. D. Gelatt, and M. P. Vecchi, Science **220**, 671 (1983).
[41] S. Kirkpatrick, J. Stat. Phys. **34**, 975 (1984).
[42] I. L. Bogolubsky, G. Burgio, M. Muller-Preussker, and V. K. Mitrjushkin, Phys. Rev. D **74**, 034503 (2006).
[43] I. L. Bogolubsky, V. G. Bornyakov, G. Burgio, E. M. Ilgenfritz, M. Muller-Preussker, and V. K. Mitrjushkin, Phys. Rev. D **77**, 014504 (2008); **77**, 039902(E) (2008).

[44] J. Greensite, S. Olejnik, and D. Zwanziger, J. High Energy Phys. 05 (2005) 070.
[45] C. Hughes, D. Mehta, and J.-I. Skullerud, Ann. Phys. (Amsterdam) **331**, 188 (2013).
[46] D. Mehta and M. Schröck, Phys. Rev. D **89**, 094512 (2014).
[47] Y. Nakagawa, A. Nakamura, T. Saito, and T. Toki, Mod. Phys. Lett. A **23**, 2348 (2008).
[48] A. Voigt, E. M. Ilgenfritz, M. Muller-Preussker, and A. Sternbeck, Phys. Rev. D **78**, 014501 (2008).
[49] J. Greensite, Phys. Rev. D **80**, 045003 (2009).
[50] H. Vogt, G. Burgio, M. Quandt, and H. Reinhardt, *Proc. Sci.*, LATTICE20132014 (2014) 363.
[51] U. Villa and S. Akle, http://web.stanford.edu/group/SOL/software/minres/ (2012).
[52] C. C. Paige and M. A. Saunders, SIAM J. Numer. Anal. **12**, 617 (1975).
[53] E. Marinari, M. L. Paciello, G. Parisi, and B. Taglienti, Phys. Lett. B **298**, 400 (1993).
[54] J. Greensite and S. Olejnik, Phys. Rev. D **67**, 094503 (2003).
[55] A. Barresi, G. Burgio, M. D'Elia, and M. Muller-Preussker, Phys. Lett. B **599**, 278 (2004).
[56] G. Burgio, M. Fuhrmann, W. Kerler, and M. Muller-Preussker, Phys. Rev. D **74**, 071502 (2006).
[57] G. Burgio, M. Fuhrmann, W. Kerler, and M. Muller-Preussker, Phys. Rev. D **75**, 014504 (2007).
[58] G. Burgio and H. Reinhardt, Phys. Rev. D **91**, 025021 (2015).
[59] A. Barresi, G. Burgio, and M. Muller-Preussker, Phys. Rev. D **69**, 094503 (2004).
[60] A. Barresi and G. Burgio, Eur. Phys. J. C **49**, 973 (2007).